Simulation of GNSS Satellite Availability in Urban Environments Using Google Earth

Taro Suzuki, Nobuaki Kubo, *Tokyo University of Marine Science and Technology, Tokyo, Japan*

BIOGRAPHIES

Taro Suzuki is a JSPS (Japan Society for the Promotion of Sciences) postdoctoral fellow at Tokyo University of Marine Science and Technology, Japan. He received his B.S., M.S., and Ph.D. in Engineering from Waseda University in 2007, 2009, and 2012 respectively. His current research interests include the GNSS precise positioning for vehicles integrated with inertial navigation and image sensors in urban environments. He is also developing the multipath mitigation techniques by the multipath simulation using 3D city models and the open source GPS software receiver. He also develops an open source software GNSS receiver library.

Nobuaki Kubo received his Master's degree of Electrical Engineering in 1998 from Hokkaido University. He received his doctorate in Engineering from University of Tokyo in 2005. He resided at Stanford University in 2008 as a visiting scholar. He is now an associate professor at the Tokyo University of Marine Science and Technology in the area of GPS/GNSS systems. His current interests are high accuracy automobile navigation using RTK and multipath mitigation techniques.

ABSTRACT

In this paper, a novel method to simulate global navigation satellite system (GNSS) satellite availability in urban environments is proposed. Owing to the increased need for positioning in urban and mountain areas, an analysis of GNSS availability and accuracy is required under conditions in which satellite visibility is low due to obstacles that block GNSS signals. The positioning accuracy depends on the number of satellites and the dilution of precision (DOP) satellite geometry. However, the DOP and actual received satellite signals depend on the surrounding environment of the GNSS antenna. The prediction of positioning accuracy and availability, which can account for the surrounding environment, such as buildings, is needed in many outdoor applications.

We therefore propose a method to directly estimate GNSS satellite visibility using Google Earth based on so-called virtual fish-eye sky image generation and without using laser scanning data or three-dimensional (3D) city models prepared in advance. Google Earth provides accurate 3D city models of many downtown areas throughout the world, even in locations where tall buildings block GNSS signals. First, a virtual image of the zenith point in the specified location is captured with Google Earth. Then, a virtual fish-eye image is generated from the nonlinear transformation of the captured image. The obstacle area in the virtual fish-eye image is extracted using a simple image binarization technique. The GNSS satellite position, which is calculated based on satellite orbit information, is projected onto the binarized fish-eye image. Satellite visibility is automatically determined by monitoring the overlapping pixels of the binarized fish-eye image.

To confirm the effectiveness of the proposed technique, a positioning test was conducted in a real-world 'urban canyon' environment. The results demonstrate that the proposed method can accurately simulate visible satellites and that the exclusion of signals from invisible satellites, which are blocked by buildings, can improve GNSS positioning availability and accuracy in urban environments.

I. INTRODUCTION

Location information is essential to outdoor applications, such as intelligent transportation systems (ITS) and pedestrian navigation. Currently, new location-based services (LBS) are being developed based on the global navigation satellite system (GNSS). GNSS is typically used for various applications to obtain an accurate self-location. These applications are usually employed in urban areas where many buildings are situated. Because of the increased need for positioning in urban areas, the prediction of GNSS performance, such as positioning accuracy and availability, is required under conditions in which satellite visibility is low due to buildings that block GNSS signals. Mobile mapping systems, for example, require the ability to carry out continuous, accurate self-positioning, even near high-rise buildings, which are especially responsible for causing multipath errors [1, 2]. The positioning accuracy depends on the number of satellites and the dilution of precision (DOP) based on the satellite geometry. However, the DOP and actual received satellite signals additionally depend on the surrounding environment of the GNSS antenna. The prediction of positioning accuracy and availability, which can account for the surrounding environment, such as buildings, is

important for planning the survey routes for mobile mapping systems.

On the other hands, in GNSS positioning, invisible satellites, which are blocked by obstacles, emit reflection and diffraction signals. These non-line-of-sight (NLOS) signals cause large positioning errors, which are also known as NLOS multipath errors [3, 4]. Urban and mountain environments include many locations where GNSS antennae receive NLOS signals from invisible satellites. The NLOS multipath error effect is highly dependent on the shape and geometry of geographic features near a GNSS receiver. Therefore, this effect cannot be addressed by differential GNSS techniques that attempt to remove most errors in GNSS positioning. For example, with fixed point GNSS observation for monitoring landslides or earthquakes [5, 6], the NLOS multipath error affects the accuracy and availability of the estimated location. Thus, estimating visible satellites and excluding NLOS signals are also important for realizing accurate and robust positioning.

In previous studies, GNSS satellite visibility has been simulated based on a well-known ray-tracing technique that employs aerial laser scanning data or existing three-dimensional (3D) city models [7-13]. Reference [9] uses a digital elevation model, which is generated from an aerial survey, to simulate satellite visibility. Reference [10] uses 3D city models and the extraction of building edges to verify satellite visibility. However, these methods based on the ray-tracing technique incur high computational costs. In addition, accurate 3D data must be prepared and modified in advance for their applications to simulate satellite visibility. Reference [13] uses the image obtained from Google Street View to estimate satellite availability. This technique is easily used; however, it can only be applied in cases where the image can be obtained from Google Street View. References [14-17] use omnidirectional or fish-eye cameras to select the visible satellites; however, they cannot be used for predicting the satellite visibility.

In this paper, we therefore propose a technique to simulate GNSS satellite visibility at any time and place in order to analyze GNSS availability and accuracy. Unlike previous studies, we present a method for directly estimating GNSS satellite visibility using Google Earth based on so-called virtual fish-eye sky image generation and without using laser scanning data or 3D city models prepared in advance.

II. METHODOLOGY

The principal concept of this study is the generation of a virtual fish-eye sky image to determine visible satellites. If the virtual fish-eye sky image can be generated in advance at a specified location, it can be repeatedly used to determine the visible satellites at a different time. Further, because the proposed method does not use the ray-tracing technique, the computational cost of this determination of visible satellites is very low. Instead, the proposed method uses the virtual fish-eye sky image and checks the satellite visibility using the satellite position projected onto the virtual fish-eye image.

The secondary concept of this study is to use Google Earth to generate the virtual fish-eye sky image. Google Earth is a free computer program that contains 3D city models generated by laser scanning data. Using Google Earth, the satellite visibility can be easily determined without using laser scanning data or 3D city models prepared in advance. In addition, Google Earth provides 3D city models of many downtown areas throughout the world. This means that the proposed method can be used at any time and place to simulate GNSS satellite availability.

Fig. 1 shows the procedures of the proposed methods. Our algorithm is executed as follows:

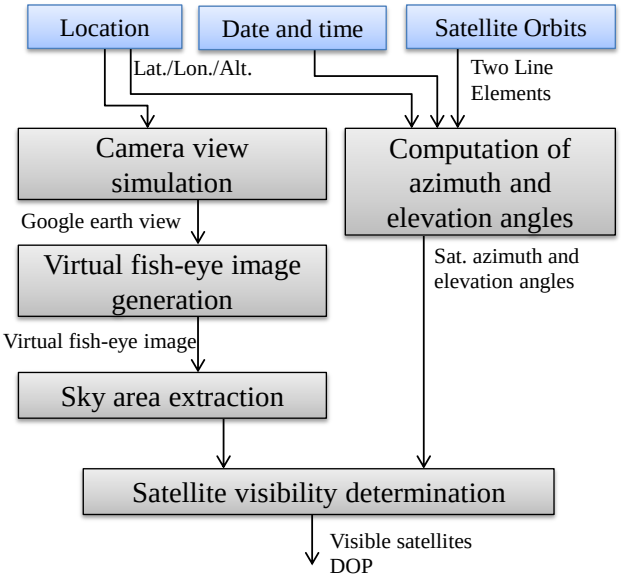

Fig.1 Proposed technique for estimating visible satellites based on the virtual fish-eye sky image.

(i) The specified location, date, time, and satellite orbit information are required for the proposed method. Here, the method employs two-line element (TLE) data for computing the satellite orbit. TLE data can be easily obtained from the Internet. The GNSS satellite azimuth and elevation angles at the input location are computed by the TLE data.

(ii) A virtual image of the zenith point in the specified location is captured through the Google Earth application programming interface (API). Here, the parameter of the

horizontal field of view of the virtual camera is configured at 180° through the API.

(iii) The camera model for the captured image from Google Earth employs a pinhole camera model. We thus convert the captured image to a fish-eye image by adding image distortion. The fish-eye image can be generated from the nonlinear transformation of the captured image.

(iv) The sky and obstacle area in the virtual fish-eye image can be extracted using a simple threshold test; the binarized fish-eye image is then generated. Finally, the GNSS satellite position is projected onto the binarized fish-eye image. Satellite visibility is automatically determined by monitoring the overlapping pixels of the binarized fish-eye image. The GNSS satellite availability, visible satellites, and DOP are outputted.

Using the proposed method, GNSS satellite visibility can be easily simulated at any time and place in order to analyze GNSS availability and accuracy. In the following section, we describe the details of the method for simulating visible satellites based on the virtual fish-eye sky image generation.

III. VIRTUAL FISH-EYE SKY IMAGE GENERATION

Unlike previous studies, we propose a method to directly estimate GNSS satellite visibility using Google Earth based on virtual fish-eye sky image generation. Google Earth provides high-resolution satellite and aerial imagery to represent the Earth as a 3D globe. As mentioned above, it additionally contains 3D city models generated by laser scanning data and provides 3D city models of many downtown areas throughout the world, even in locations where tall buildings block GNSS signals. We propose a technique to simulate GNSS satellite visibility at any time and place in order to analyze GNSS availability and accuracy using Google Earth.

In previous studies, GNSS satellite visibility is simulated based on a well-known ray-tracing technique using 3D environmental data. In general, the computational cost of determining satellite visibility from a 3D model is high because ray tracing requires extensive calculations. By contrast, when using our proposed method, the cost is very low because we use virtual fish-eye image generation based on Google Earth to determine satellite visibility. Another advantage of using Google Earth is that it contains accurate 3D city models generated from aerial laser scanning data. To simulate satellite availability, we do not need to prepare in advance the laser scanning data or 3D city models. The proposed method only requires the specific location, date and time of the simulation, and satellite orbit data to simulate satellite visibility; thus, the proposed method can be easily used for various applications.

The camera model for the captured image from Google Earth employs the pinhole camera model. The fish-eye image can be generated from the nonlinear transformation of the captured image. The pixels in the captured image in the zenith direction from Google Earth are denoted as x and y. The elevation angle el and azimuth angle az of the pixels in the image are calculated as:

$$el = \arctan\left(\frac{sqrt(x^2+y^2)}{f}\right) \quad (1)$$

$$az = \arctan\left(\frac{y}{x}\right) \quad (2)$$

where f is the focal length, which can be calculated from the horizontal field of view (HFOV) of the virtual camera and the image width w of the virtual image. These parameters can be obtained through the Google Earth API, and f is computed as:

$$f = \frac{w}{2\arctan\left(\frac{HFOV}{2}\right)} \quad (3)$$

The image width of the generated virtual fish-eye sky image is denoted as w_{fish}. The pixels in the virtual fish-eye image x_{fish} and y_{fish} are computed as:

$$x_{fish} = \frac{el}{\pi} w_{fish} cos(az) + \frac{w_{fish}}{2} \quad (4)$$

$$y_{fish} = \frac{el}{\pi} w_{fish} sin(az) + \frac{w_{fish}}{2} \quad (5)$$

Using Equations (1) to (5), the captured image from Google Earth can be converted to the fish-eye image by nonlinear transformation. The captured image and generated virtual fish-eye image are shown in Fig. 2. The captured image, which is based on the pinhole camera model, is distorted. However, the generated virtual fish-eye image directly represents the simulated environment; it therefore can be used to check the satellite visibility.

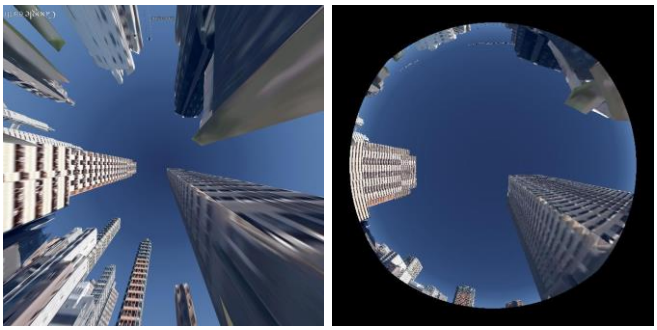

Fig.2 Simulated image from Google Earth (left) and generated virtual fish-eye image (right).

IV. SATELLITE VISIBILITY DETERMINATION

Next, we describe satellite visibility determination using the virtual fish-eye sky image. To determine the visible satellites, the sky area in the virtual fish-eye image must be extracted. Sky area extraction is performed by a simple technique. First, the fish-eye sky mask image is generated in advance from Google Earth. Fig. 3(a) shows the fish-eye sky mask image, which is simulated as an open-sky environment by the method described in the previous section. The sky area is always rendered as the same light-blue color as in the generated virtual fish-eye image. The difference image between the generated virtual fish-eye image and the sky mask image is computed to determine the sky area. The difference image is shown in Fig. 3(b); the difference of image intensity values is almost zero in the sky area. A simple threshold test is used to generate the binarized fish-eye image. The sky area in the simulated virtual fish-eye sky image can be easily and robustly detected by the proposed method.

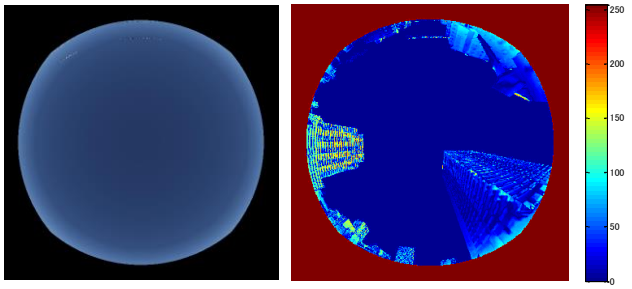

Fig.3 Sky area extraction using the fish-eye sky mask image.

Next, we describe the projection of the satellite position onto the binarized fish-eye image. First, we calculate the satellite position in local east, north, up (ENU) coordinates with the origin at the location where the fish-eye image is generated. The satellite position, $x_{sat,ECEF}$, $y_{sat,ECEF}$, $z_{sat,ECEF}$, in Earth-centered Earth-fixed (ECEF) coordinates can be calculated from the TLE data. To transform the ECEF coordinates into local ENU coordinates, the following equations are used:

$$\begin{bmatrix} x_{sat,ENU} \\ y_{sat,ENU} \\ z_{sat,ENU} \end{bmatrix} = \mathbf{C}_{ECEF}^{ENU} \begin{bmatrix} x_{sat,ECEF} - x_{0,ECEF} \\ y_{sat,ECEF} - y_{0,ECEF} \\ z_{sat,ECEF} - z_{0,ECEF} \end{bmatrix} \quad (6)$$

$\mathbf{C}_{ECEF}^{ENU}$ is the rotation matrix denoted as:

$$\mathbf{C}_{ECEF}^{ENU} = \begin{bmatrix} -\sin\lambda_0 & \cos\lambda_0 & 0 \\ -\sin\varphi_0\cos\lambda_0 & -\sin\varphi_0\sin\lambda_0 & \cos\varphi_0 \\ \cos\varphi_0\cos\lambda_0 & \cos\varphi_0\sin\lambda_0 & \sin\varphi_0 \end{bmatrix} \quad (7)$$

Here, x_0, y_0, z_0, λ_0, and φ_0 are the input location in the ECEF and geodetic coordinates, respectively. The satellite position is converted into the azimuth az_{sat} and elevation el_{sat} angles as follows:

$$az_{sat} = \arctan(y_{sat,ENU} / x_{sat,ENU}) \quad (8)$$

$$el_{sat} = \arctan(z_{sat,ENU} / \sqrt{x_{sat,ENU}^2 + y_{sat,ENU}^2}) \quad (9)$$

The satellite positions are plotted to determine the visibility of each satellite from the overlapping of the satellites and sky area. The visibility of the satellite is easily determined by checking the value of the pixels in the binarized fish-eye image of its position. The process of determining the visible satellites is automatically performed. Using the described method, GNSS satellite visibility can be automatically simulated at any time and place from Google Earth.

V. EXPERIMENTS

To confirm the effectiveness of the proposed method, two positioning tests—static and kinetic—were conducted in a real 'urban canyon' environment. In these tests, we evaluated the accuracy of the visible satellite simulation by the proposed method and the effectiveness of the NLOS signal extraction by the virtual fish-eye sky image.

A. Static test

A static test was performed on February 23 and 24, 2015 at a known location in the Yaesu area of Tokyo, Japan, where many buildings are situated. The two locations of the static test are shown in Fig. 4. The GNSS antenna (Trimble Zephyr 2) and GNSS receiver (Trimble NetR9) were used to collect the GNSS data at a rate of 1 Hz over a 12-hr period.

First, we generated virtual fish-eye sky images using the proposed method and compared them with the actual images captured by the fish-eye camera. The actual captured images are shown in Fig. 5; the simulated virtual fish-eye sky images are shown in Fig. 6. Note that the intrinsic parameters of the actual fish-eye camera (shown in Fig. 5) were not calibrated. Thus, the relationship between the elevation angle and pixel location in the actual fish-eye camera was not linear. However, from these figures, we could verify that the appearances of the actual and simulated fish-eye images were almost the same, and that the proposed method could accurately simulate sky images from Google Earth. Fig. 7 shows the result of the sky area extraction from the generated virtual fish-eye sky image. The red area in the figure indicates the extracted sky area. Compared with the simulated virtual fish-eye sky images in Fig. 6, the sky area extraction shown in Fig. 7 was successfully performed.

Fig.4 Static test environment (Yaesu area, Tokyo, Japan).


Fig.5 Fish-eye image in Test #1 (left) and Test #2 (right).

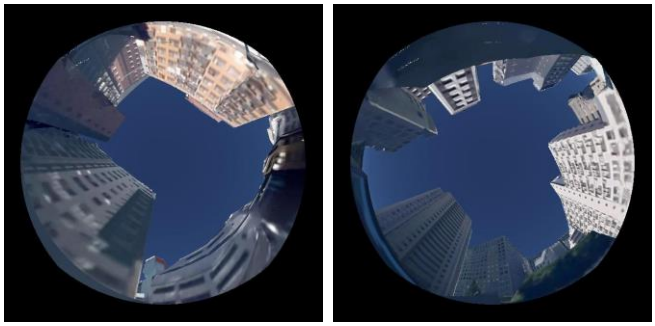
Fig.6 Simulated virtual fish-eye sky image in Test #1 (left) and Test #2 (right).

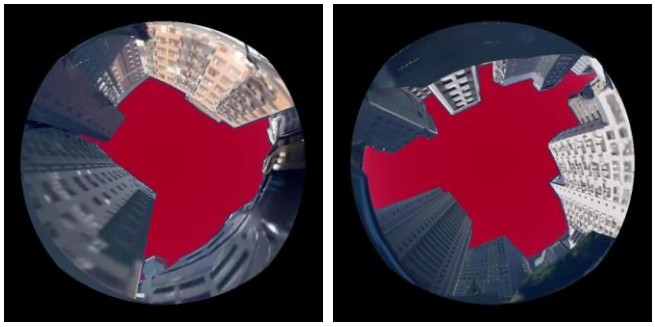
Fig.7 Extraction of the sky area (red) in Test #1 (left) and Test #2 (right).

At this point, we compared the simulated GNSS satellite visibility and actual received GNSS signals of the static test. Fig. 8 illustrates the success rate of the visible satellite simulation over a 12-hr period. The blue area in Fig. 8 indicates that the simulated visible satellites matched the actual received signals; the red area indicates that the simulated visible satellites were mismatched. Most of the simulated and actual GNSS satellites matched. The total success rates of the visible satellite simulations were 96.37% in Test 1 and 95.69% in Test 2. The numbers of received satellite and simulated satellite signals in the given time interval are shown in Fig. 9. The blue and red lines respectively indicate the actual and simulated numbers of satellites. The changes of both numbers of satellites were almost the same; however, the total number of satellites in the simulation was smaller than the actual number of satellites because we received NLOS multipath signals from invisible satellites that were blocked by buildings in the actual urban environment. It can be inferred that, if these multipath signals were to be excluded, the GNSS positioning availability and accuracy in the static survey would be improved.

Finally, we excluded the NLOS signals from the observed GNSS signals by means of the proposed method and then compared the positioning results. Fig. 10 illustrates the actual received GNSS signals projected onto the virtual fish-eye sky image. We verified that the many NLOS multipath signals were received from invisible satellites.

We compared the results of the two positioning methods: the normal real-time kinematic (RTK)-GNSS positioning result from using the threshold of the GNSS signal-to-noise ratio (SNR) (35 dB/Hz), and the satellite exclusion from using the virtual fish-eye sky image. It should be noted that, under multipath conditions, the SNR often decreases because signals decay from diffraction and reflection. The SNR threshold is typically used to reduce multipath errors. The result of position estimation in our test is shown in Fig. 11. The blue and red points respectively indicate the before and after states of NLOS signal exclusion by the proposed method. Table 1 shows the horizontal root mean square (RMS) error, maximum error, and availability of the fixed solutions of RTK-GNSS. The positioning accuracy of the excluded NLOS signals was slightly improved compared to that without exclusion. In contrast, the availability of the RTK-GNSS fixed solutions was greatly improved from 20.36% to 51.20% in Test 1, and from 35.75% to 68.02% in Test 2. It is evident that the proposed method can improve the accuracy and availability of the GNSS fixed-point observation.

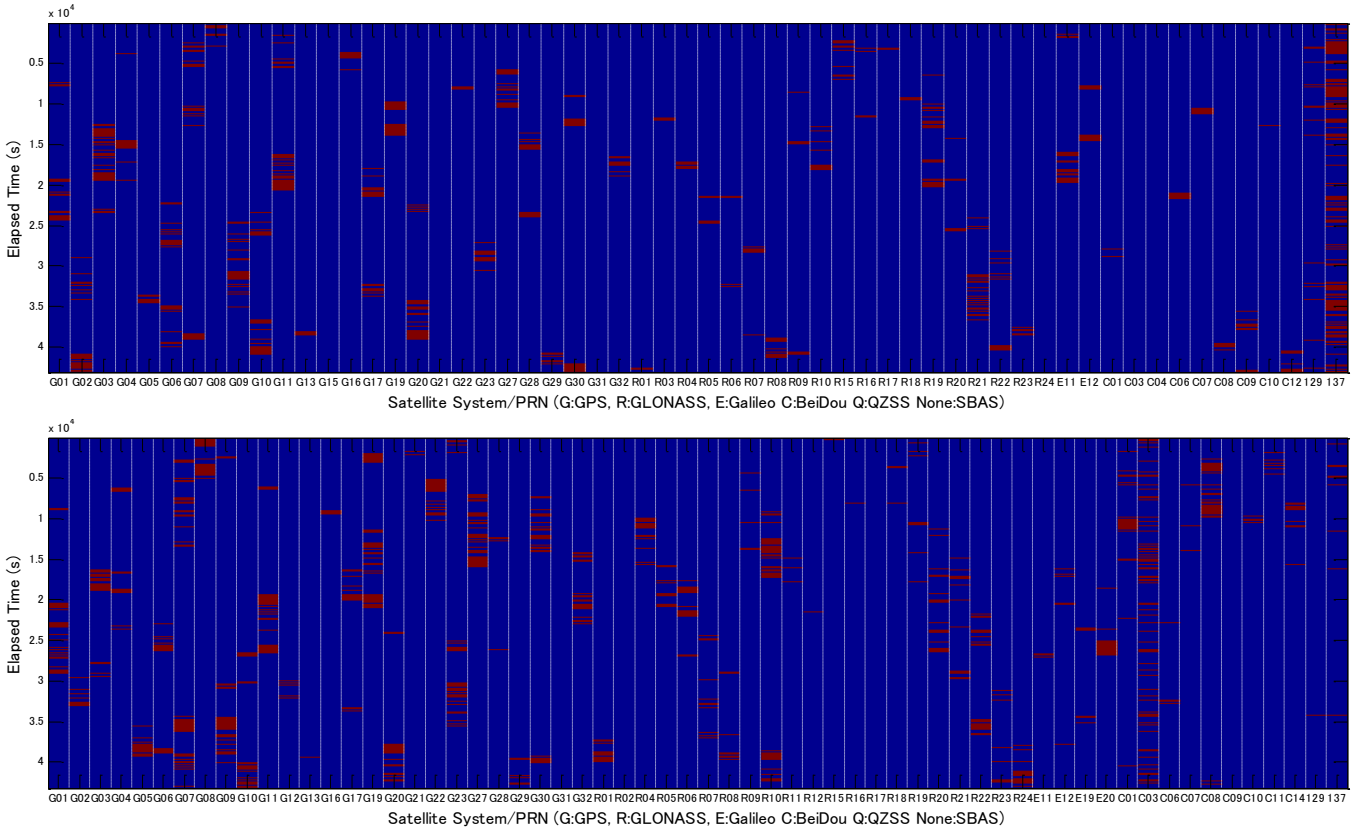

Fig.8 Evaluation of the success rate of the visible satellite simulation in Test #1 (top) and Test #2 (bottom). Blue and red respectively indicate the matching and mismatching of simulated satellite visibility.

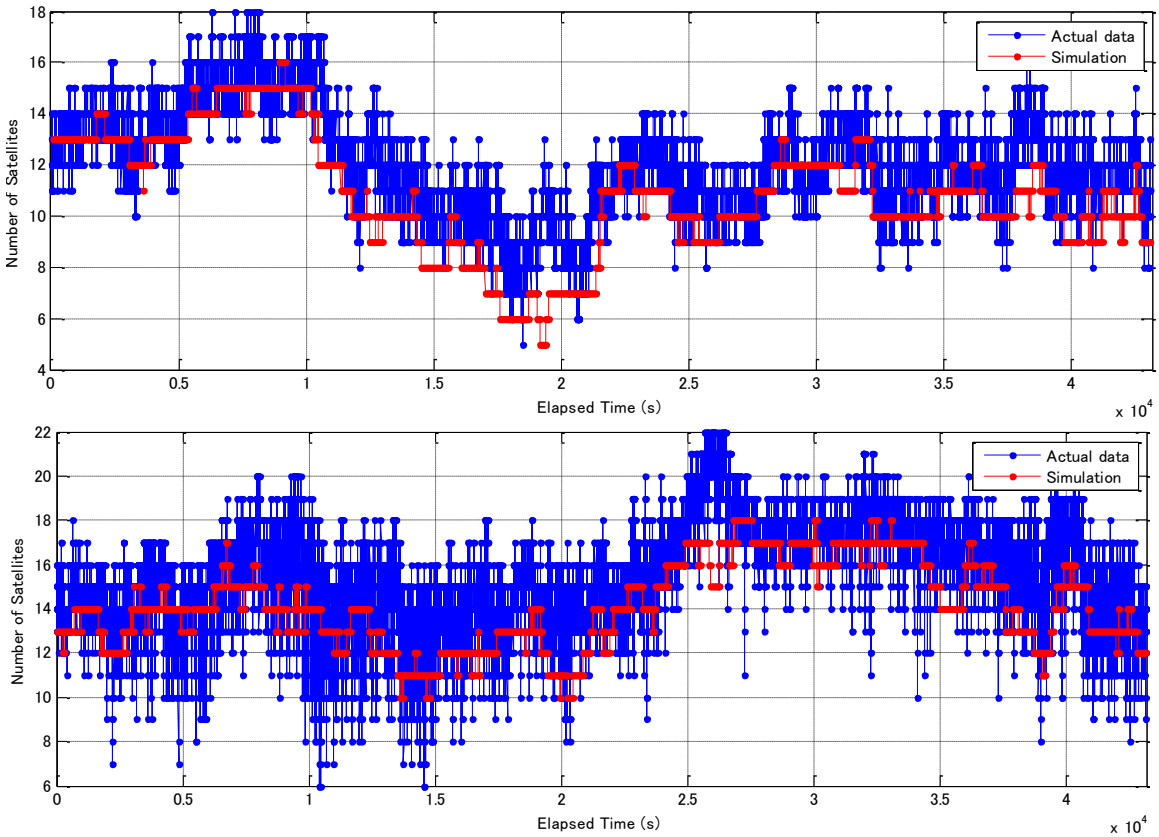

Fig.9 Comparison of the number of received and simulated satellite signals in Test #1 (top) and Test #2 (bottom).

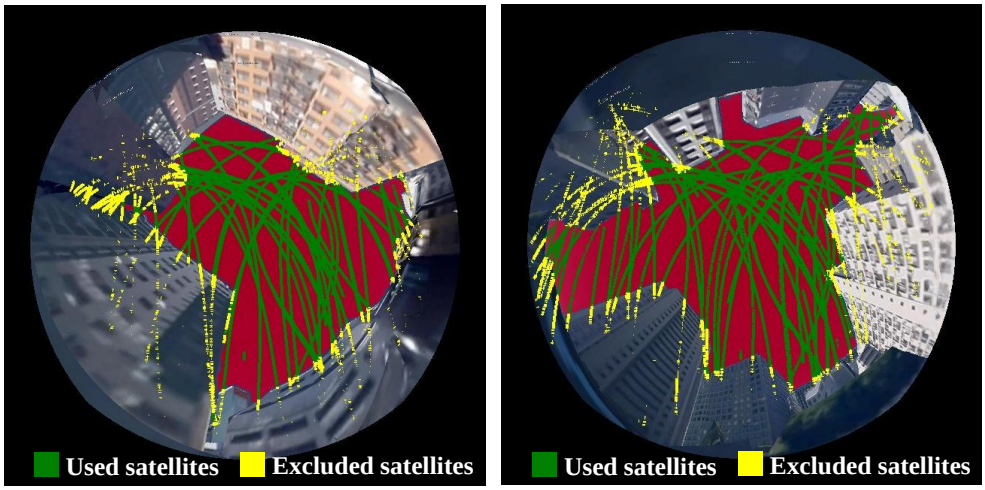

Fig.10 Visible satellites selection from the virtual fish-eye sky image in Test #1 (left) and Test #2 (right).

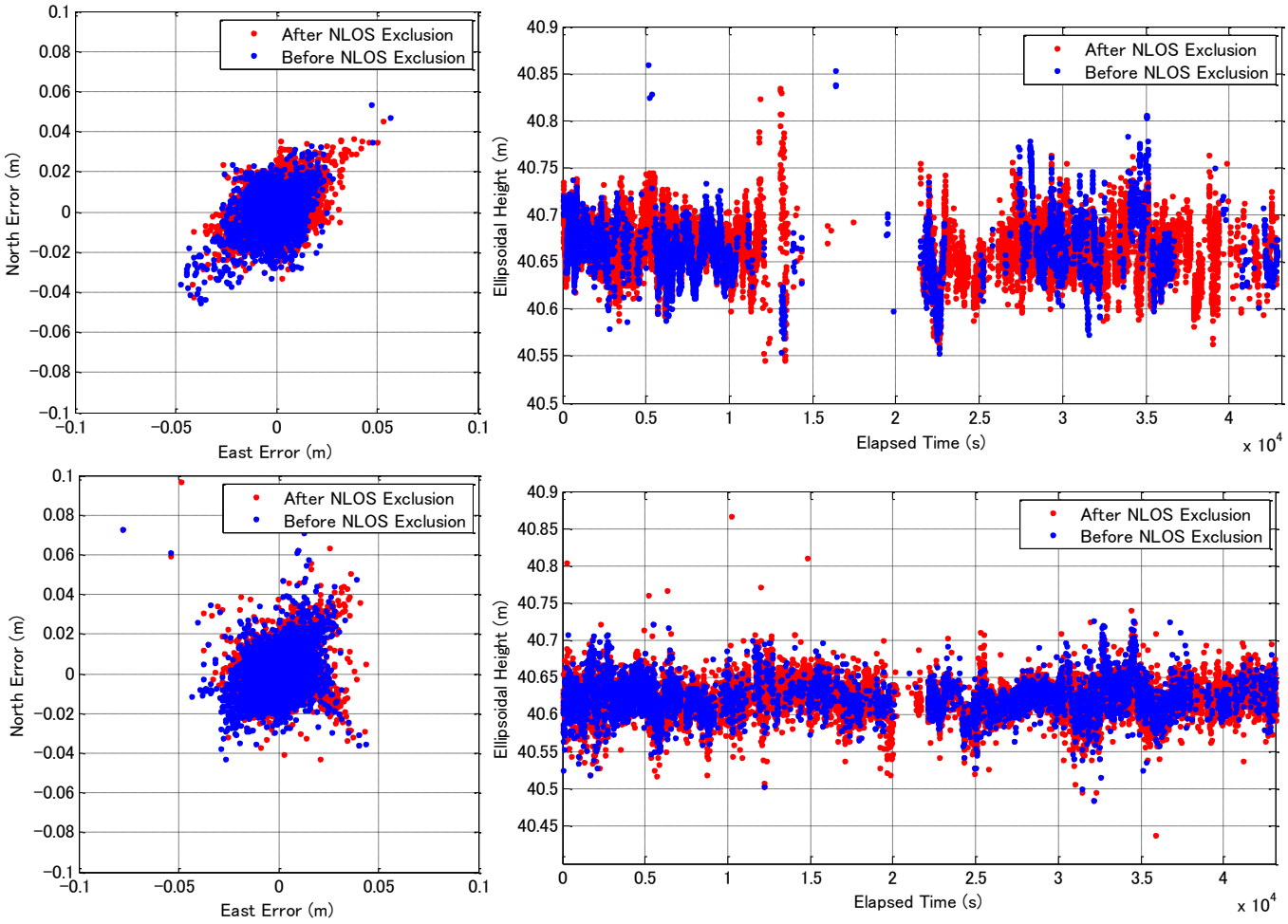

Fig.11 Comparison of position accuracy before and after satellite exclusion in Test #1 (top) and Test #2 (bottom).

Table 1 Result of horizontal positioning errors

	Test #1		Test #2	
	Before NLOS exclusion	After NLOS exclusion	Before NLOS exclusion	After NLOS exclusion
RMS error	1.25 cm	1.17 cm	1.21 cm	1.10 cm
Maximum error	7.36 cm	6.99 cm	10.67 cm	10.84 cm
Availability	20.36 %	51.20 %	35.75 %	68.02 %

B. Kinetic test

A kinematic positioning test was performed on October 17, 2013 in the Tsukishima area of Tokyo, Japan, where many buildings are located. The travel route is shown in Fig. 12. The round-trip travel route was approximately 3 km. The travel route surroundings included many buildings; it was therefore an environment susceptible to satellite masking. A GNSS antenna and a fish-eye camera were installed on the roof of a vehicle, and GNSS data and fish-eye images were then collected from the urban environment. The reference position and orientation of the vehicle were computed using a high-grade gyroscope and GNSS integration system as a ground truth.

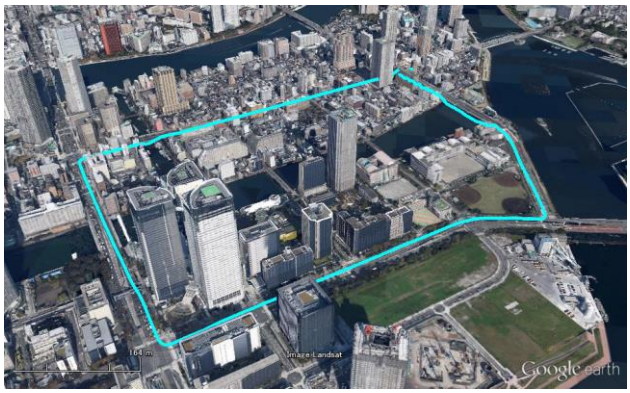

Fig.12 Kinetic test environment and path (Tsukishima area, Tokyo, Japan).

The actual fish-eye images captured during the test, the simulated virtual fish-eye images, and the results of the sky area extraction by the proposed method are shown in Fig. 13. The simulated GNSS satellites were projected onto the virtual fish-eye images; the circle and cross markers in Figs. 13(b) and (c) respectively indicate the visible and invisible satellites determined by the proposed method. Based on this result, we verify that the proposed technique can accurately simulate the sky images and visible satellites.

Next, we compared the number of actual received satellite and simulated satellite signals. Fig. 14 shows the number of satellites in a time series. The actual and simulated numbers of satellites were almost the same, and the average numbers of satellites in the actual data and simulation were 13.48 and 13.82, respectively. The success rate of the visible satellite simulation was 90.84%.

We compared the RTK-GNSS positioning results by using the threshold of the GNSS SNR (35 dB/Hz); in addition, we compared the satellite exclusions by using the virtual fish-eye sky images, as with the static test. The positioning estimation results are shown in Fig. 15. The blue and red points respectively indicate the before and after states of the NLOS signal exclusion by the proposed method. From the data in Fig. 15, the new fixed solution could be generated in the case of using NLOS signal extraction. The availability of the RTK-GNSS fixed solutions improved from 59.76% to 69.02%.

These results demonstrate that the proposed technique can accurately simulate GNSS satellite visibility without using laser scanning data or 3D city models prepared in advance. Moreover, predicting GNSS availability by the proposed method is effective and useful for many outdoor applications, such as ITS and survey applications.

VI. CONCLUSION

GNSS is typically used for various applications to obtain an accurate self-location; these applications are usually employed in urban areas where many buildings are located. Thus, estimating GNSS positioning availability and accuracy in urban areas is needed for these applications, such as those for ITS and surveying. In this paper, we proposed a method to estimate GNSS satellite visibility using Google Earth based on virtual fish-eye sky image generation. A virtual fish-eye sky image is generated from the view captured from Google Earth using nonlinear transformation. The visible satellites are automatically determined based on sky area extraction of the virtual fish-eye image. Our method can easily and robustly simulate satellite visibility without using laser scanning data or 3D city models prepared in advance. Moreover, the computational cost of the proposed method is very low, and it can be used at any time and place throughout the world.

To evaluate the proposed method, static and kinematic evaluations were performed in urban environments. The results demonstrate that the proposed method can accurately simulate visible satellites and that the exclusion of NLOS signals determined by the proposed method can improve GNSS positioning availability and accuracy. From these results, it is evident that prediction of GNSS availability by the proposed method is effective and useful for ITS and survey applications.

ACKNOWLEDGMENTS

This work was supported by Grant-in-Aid for Japan Society for the Promotion of Science (JSPS) Fellows.

REFERENCES

[1] N. El-Sheimy and K. P. Schwarz, “Navigating Urban Areas by VISAT—A Mobile Mapping System Integrating GPS/INS/Digital Cameras for GIS Applications,” Journal of the Institute of Navigation, vol. 45, no. 4, pp.275 -285, 1998.

[2] C. Ellum, N. El-Sheimy, “Land-based mobile mapping systems,” Photogrammetric Engineering and Remote Sensing, 68 (1), pp. 13–17, 2002.

(a) Fish-eye images and actual received signals

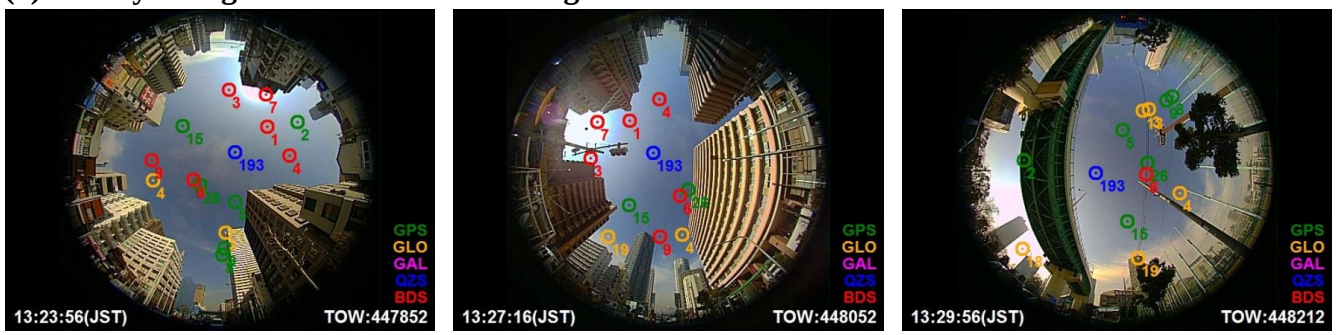

(b) Virtual fish-eye images and simulated satellites

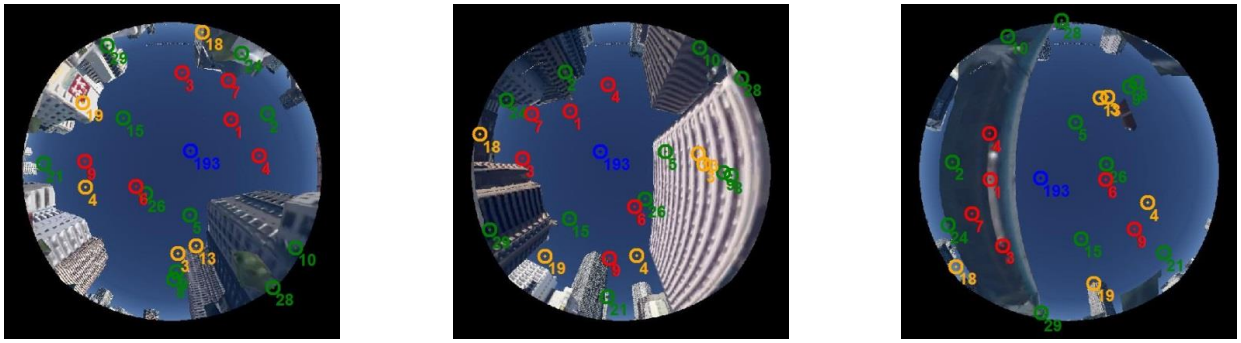

(c) Sky-area detection results and simulated visible satellites

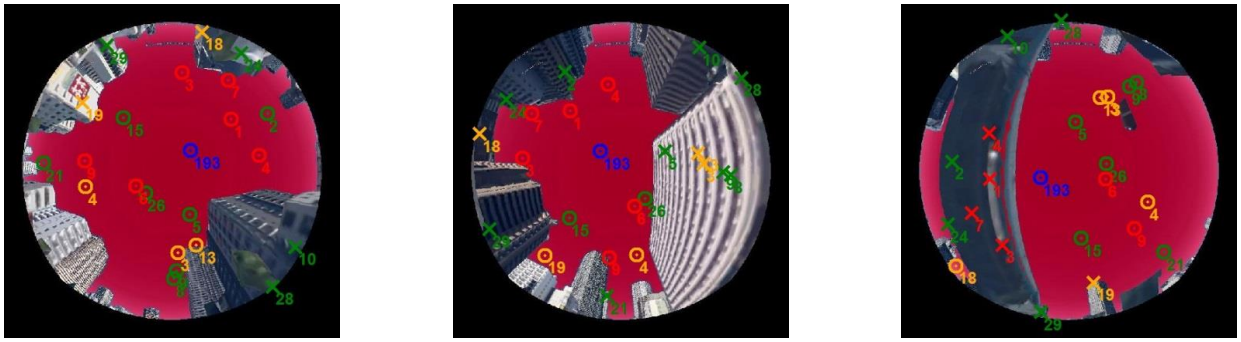

Fig.13 Actual fish-eye image, virtual fish-eye sky image, and visible satellites extraction in the kinetic test.

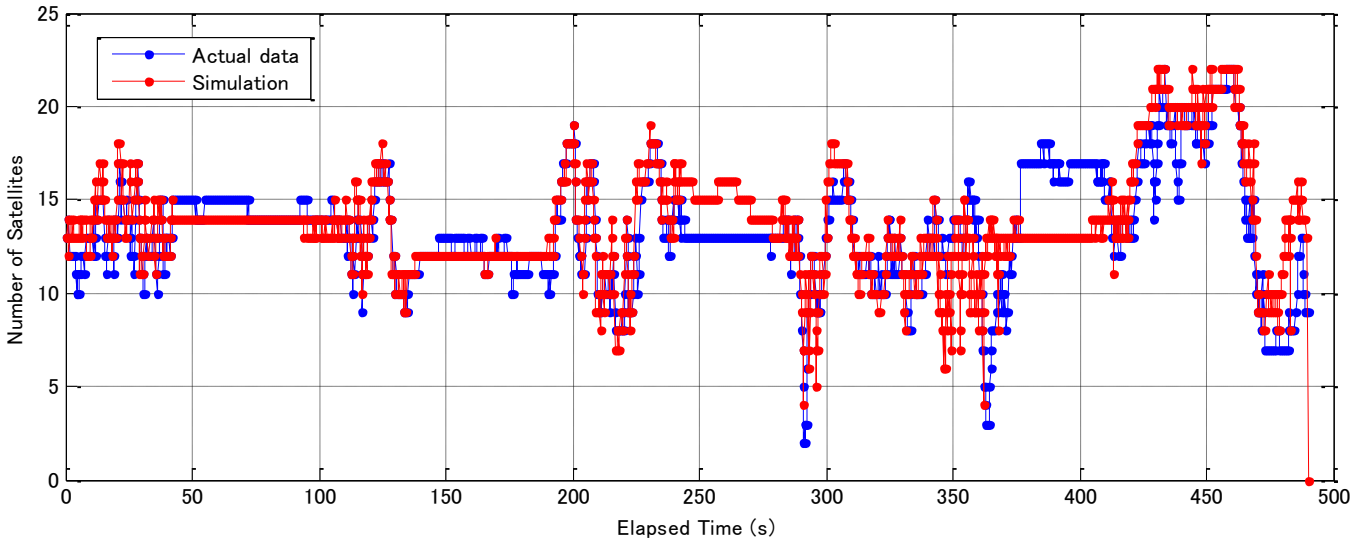

Fig.14 Comparison of the number of received and simulated satellite signals.

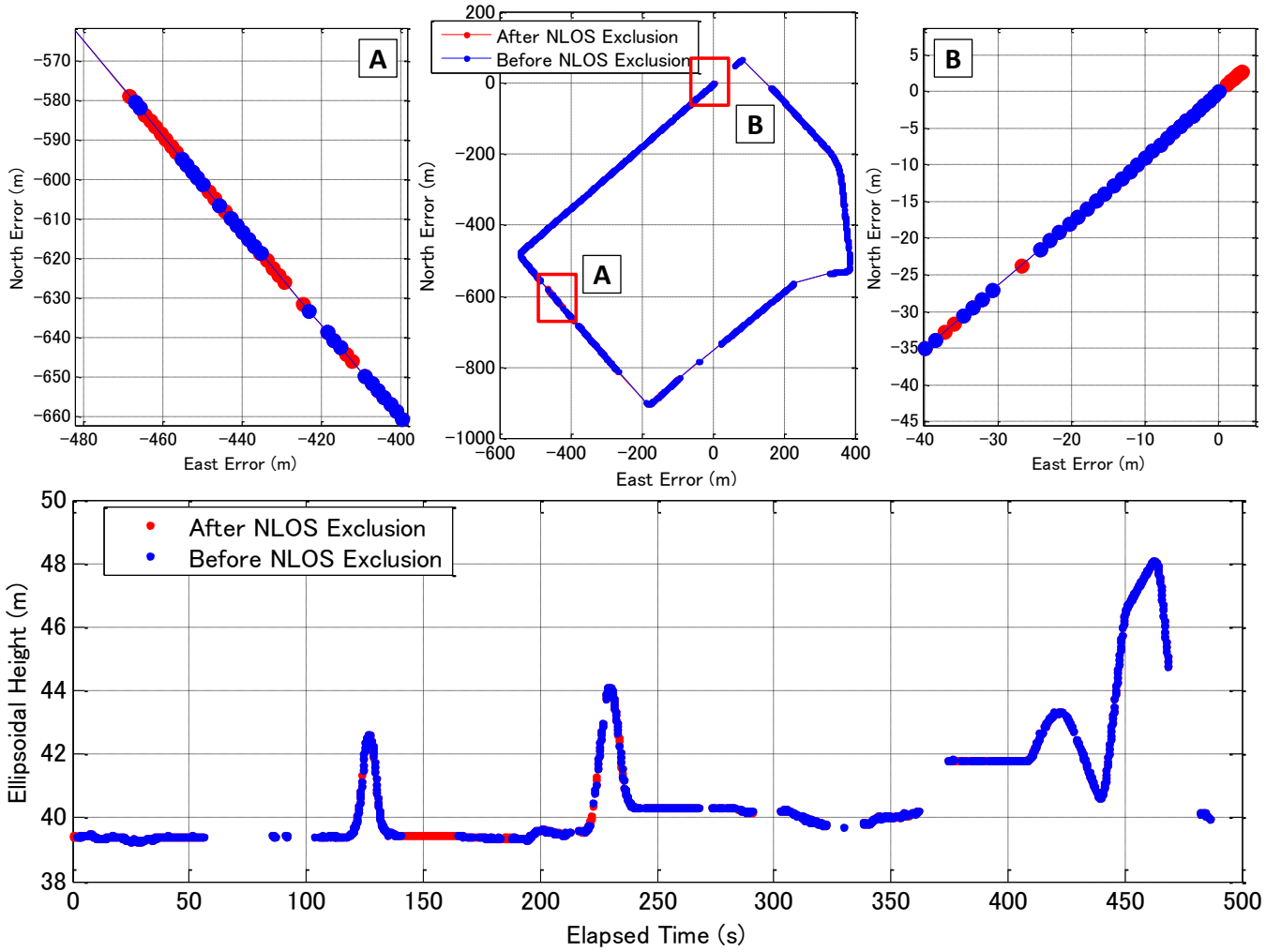

Fig.15 Comparison of position accuracy before and after satellite exclusion.

[3] Soubielle, J., et al., "GPS positioning in a multipath environment," IEEE Transactions on Signal Processing, vol. 50, pp. 141-150, 2002.

[4] Paul D. Groves, et. al, "A Portfolio Approach to NLOS and Multipath Mitigation in Dense Urban Areas," Proc. of ION GNSS 2013, pp. 3231-3247, 2013.

[5] J. Coe, W. Ellis, J. Godt, W. Savage, J. Savage, J. Michael, J. Kibler, P. Powers, D. Lidke, S. Debray, "Seasonal movement of the Slumgullion landslide determined from Global Positioning System surveys and field instrumentation, July 1998–March 2002," Engineering Geology, 68, pp. 67–101, 2003.

[6] Wang G., "GPS Landslide Monitoring: Single Base vs. Network Solutions - A case study based on the Puerto Rico and Virgin Islands Permanent GPS Network," Journal of Geodetic Science, 1, 191-203, 2011.

[7] Kleijer, F., and D. Odijk and E. Verbree, "Prediction of GNSS Availability and Accuracy in Urban Environments - Case Study Schiphol Airport," Chapter 23 of Location Based Services and TeleCartography II In: REHRL, G. G. A. K. (ed.). Springer-Verlag, Berlin Heidelberg, 2009.

[8] Taylor, G., Li., J., Kidner, D.B., Brunsdon, C., Ware, J.M., "Modelling and Prediction of GPS Availability with Digital Photogrammetry and LiDAR," The International Journal of Geographical Information Science, 2007.

[9] Costa, E., "Simulation of the Effects of Different Urban Environments on GPS Performance Using Digital Elevation Models and Building Databases," Transactions on Intelligent Transportation Systems, Vol. 12, pp. 819-829, 2011.

[10] Groves, P. D., "Shadow Matching: A New GNSS Positioning Technique for Urban Canyons," The Journal of Navigation, Vol. 64, pp. 417-430, 2011.

[11] Taro Suzuki, Nobuaki Kubo, “GNSS Positioning with Multipath Simulation using 3D Surface Model in Urban Canyon,” The 25th International Technical Meeting of The Satellite Division of the Institute of Navigation (ION GNSS 2012), 2013., pp.438-447, 2012.

[12] Taro Suzuki, Nobuaki Kubo, “Correcting GNSS Multipath Errors Using a 3D Surface Model and Particle Filter,” The 26th International Technical Meeting of The Satellite Division of the Institute of Navigation (ION GNSS 2013), 2013.

[13] Sakpod Tongleamnak, et al., “Simulation of GNSS Satellite Visibility in Urban Area Using Google Street View,” 6th Asia Oceania Regional Workshop on GNSS, 2014.

[14] J. Marais, M. Berbineau, and M. Heddebaut, “Land mobile GNSS availability and multipath evaluation tool,” Vehicular Technology, IEEE Transactions on, vol. 54, no. 5, pp. 1697–1704, 2005.

[15] Meguro, J., et al., “GPS Multipath Mitigation for Urban Area Using Omnidirectional Infrared Camera,” IEEE Transactions on Intelligent Transportation Systems, Vol. 10, No. 1, pp. 22-30, 2009.

[16] Taro Suzuki, et. al, “Multipath Mitigation Using Omnidirectional Infrared Camera for Tightly Coupled GPS/INS Integration in Urban Environment,” Proc. of ION GNSS 2011, pp.2914-2922, 2011.

[17] Taro Suzuki, Nobuaki Kubo, “N-LOS GNSS Signal Detection Using Fish-Eye Camera for Vehicle Navigation in Urban Environments,” The 27th International Technical Meeting of The Satellite Division of the Institute of Navigation (ION GNSS 2014), 2014.